# CORRECTION OF $B_0$ INHOMOGENEITY DISTORTION IN MAGNETIC RESONANCE SPECTROSCOPIC IMAGING

*Ramin Eslami and Mathews Jacob*

Department of Biomedical Engineering, University of Rochester, Rochester, NY 14627

## ABSTRACT

In this paper we reconstruct the 3-D MR spectroscopic data acquired using an *echo-planar spectroscopic imaging* (EPSI) sequence. We propose to compensate for $B_0$ inhomogeneity artifact by using the $B_0$ field map and $T_2^*$ decay estimated from a higher resolution, multi-slice proton imaging data scanned with similar shimming to the EPSI one. We employ *total variation* (TV) regularization to obtain more uniform spectral peaks and lineshapes, and exploit the sparsity of the spectral data by using the $\ell_1$ norm in the reconstruction.

***Index Terms—*** $B_0$ inhomogeneity compensation, magnetic resonance spectroscopic imaging

## 1. INTRODUCTION

The difference between MRI and *MR spectroscopic imaging* (MRSI) is the inclusion of time domain (or equivalently the spectral domain) to the spatial MR data in MRSI. Hence, MRSI serves as a useful means to measure concentrations of various in vivo metabolites, which are crucial in diagnosis of a variety of diseases.

In a MR scanner, acquiring perfectly homogenous $B_0$ field is impossible; hence, some artifacts are introduced in the imaging data due to field inhomogeneity. In MRSI, to ensure that reconstructions have good *signal to noise ratio* (SNR) in a specified acquisition time, imaging is conducted at low spatial resolution (e.g. 32x32). The effect of $B_0$ field inhomogeneity coupled with the low resolution acquisition lead to increased $T_2^*$ decay and distorted line shapes. At each voxel $\mathbf{r}=(x,y,z)\in\Omega$ in a water phantom, the FID (*free induction decay*) signal in the presence of field inhomogeneity $\Delta B_0(\mathbf{r})$ is

$$s(t) \simeq \int_{\mathbf{r}\in\Omega} \rho_0 e^{-j\gamma\Delta B_0(\mathbf{r})t} e^{-t/T_2} d\mathbf{r}\,, \qquad (1)$$

where $\gamma$ denotes the gyromagnetic ratio and $\rho_0$ is a constant. As (1) shows, for a larger voxel size $\Omega$, the contribution of $e^{-j\gamma\Delta B_0(\mathbf{r})t} \triangleq e^{-j\phi(\mathbf{r})t}$ is more pronounced resulting in higher $T_2^*$ decay. Therefore, in MRSI it is imperative to compensate for $e^{-j\phi(\mathbf{r})t}$, which is a frequency shift in the spectral domain, from each voxel to obtain a more reliable spectroscopic data.

We can mention to [2], [5], [6] as some of the related studies. The main contributions of the paper are listed below.

- What mainly distinguishes our work from the others is taking advantage of a higher resolution field map in *multiple slices.*
- We take into account the $T_2^*$ decay estimated from high resolution data.
- We benefit from the sparsity of the spectral data as a prior knowledge in reconstruction and thus employing $\ell_1$ norm.
- Our approach provides a useful practical tool for real imaging applications.

*Notations:* We denote each image acquired at each echo a frame. In the discrete domain we denote spatial indices by $\mathbf{n}=[n_x,n_y,n_z]$ and $n_t$ as the time index (or frame). In the frequency domain, we denote the corresponding discrete frequencies as $\mathbf{k}=[k_x,k_y,k_z]$ and $k_t$ (and $\omega_t$ as the continuous version of $k_t$). We represent the MRS signal as $s[n_x,n_y,n_t]$ in time and $s_{(t)}[n_x,n_y,k_t]$ in the spectral domain. In general, we denote $s_{(x)}$ as the DFT of $s$ along $n_x$ or $s_{(x)}=\mathcal{F}_{(x)}s$ and $s_{(xy)}$ the 2-D DFT of $s$ along $n_x$ and $n_y$, and so on.

## 2. PRELIMINARIES

We use *echo-planar spectroscopic imaging* (EPSI) sequence to acquire MRSI data. Before reconstruction, we need to discuss challenges related to MRSI.

### 2.1. Acquisition

We designed an EPSI sequence to acquire the MRS data in a Cartesian grid from a uniform phantom containing water, choline (Cho), creatine (Cr), and N-acetyl-aspartate (NAA). We scanned the phantom for a proton image as well as metabolite image explained below.

- We scanned the phantom for metabolites using water suppression where we used 7 repetitions at resolution $(\mathbf{M},M_t)=(M_x,M_y,N_t)=(32,32,128)$ to have a higher SNR. The volume has 32x32 image resolution in 1 slice (10mm thick) and 128 instants of time (echoes) with a frequency of about 1kHz. We denote this scan as $s_{0(xy)}[k_x,k_y,n_t]$
- We also scanned the phantom for water image with the same resolution.
- To estimate the inhomogeneity field map $\phi[\mathbf{n}]$, we need a finer-resolution proton scan (in addition to the low-resolution MRSI) to ensure a more accurate estimate with low $T_2^*$ decay distortion. As a result, we scanned the same

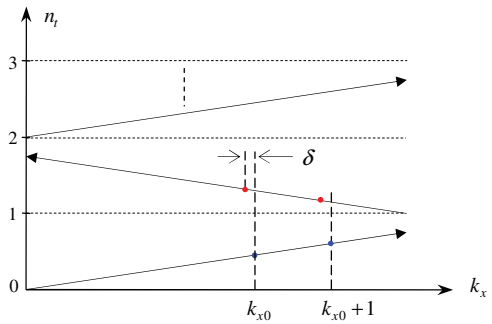


Fig. 1. Zigzag scanning trajectory of EPSI. The shift between even and odd lines is shown with $\delta$ at a typical point $n_x = n_{x0}$.

volume with $\mathbf{N} = (N_x, N_y, N_z) = (64,64,4)$ resolution (4 slices; 2.5mm each) and acquired data with 4 echoes corresponding to frames 0, 2, 4, and 80. We denote the high-resolution scan as $s_{1(xy)}[k_x, k_y, n_z, n_t]$. The need for multiple echoes is to phase-unwrap the field map estimate as explained in Section 2.3.

### 2.2. Shift between Even and Odd Samples

Fig. 1 illustrates the zigzag scanning trajectory we use in the EPSI for a fixed $[k_y, n_z]$ point. One of the drawbacks of EPSI in a zigzag scanning is the introduction of a shift in sampling locations along $k_x$ between even and odd frames [1], which is indicated by $\delta$ in this figure. This distortion yields an artificial peak at $\omega_t = \pi$ from the water spectral peak. We use an algorithm based on linear estimation to compensate for this shift in the spectroscopic data. We denote the corrected data as $s[n_x, n_y, n_t]$.

In addition to the above issue, in zigzag scanning the acquired *k*-space points are not in the Cartesian grid. In this paper we approximate the zigzag scanning with a uniform grid discretized in time as shown by dashed horizontal lines in Fig. 1. That is $n_t = \lfloor 2t/T \rfloor$ where $T$ is the period equal to the sum of a positive and a negative echo which we assume they have equal length.

### 2.3. Field Map Estimation

As mentioned in Section 2.1, to estimate the field map we acquire a secondary higher resolution proton imaging data in several frames from the same volume used for spectroscopic imaging.

Field map estimation is usually done based on two frames where we have $\phi_J[\mathbf{n}] = J^{-1}\angle(s_1[\mathbf{n}, J]/s_1[\mathbf{n}, 0])$ [3]. Here we use frame 0 and frame $J$ (an even frame to avoid the shift adjustment mentioned in Section 2.2). If one chooses the $J$ th frame to be too close to the 0th one, $\phi_J$ will be noisy and for larger values of $J$, we encounter phase wrapping in the estimation.

To correct for the phase wrap for an estimate $\phi_{J_2}$, we use a different field estimation $\phi_{J_1}$ (with no phase wrap) as reference. Fig. 2 shows the original and the corrected field map $80\phi_{80}$. We use $\phi$ for $\phi_{80}$ henceforth.

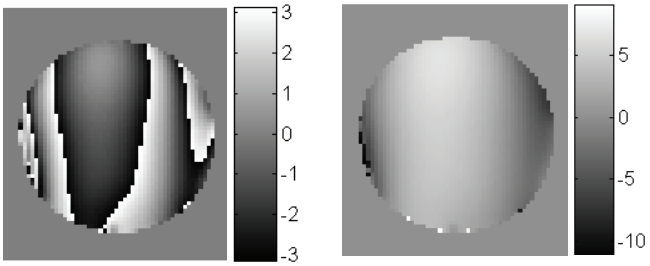


Fig. 2. *Left:* Field map of $80\phi_{80}$. *Right:* Corrected field map of $80\phi_{80}$ shown in bottom.

In addition to estimating the field map, we also estimate $T_2^*$ from the high-resolution data. Note that for a very high resolution scan, $T_2^* \simeq T_2$. We use a time-invariant estimation as $T_2^*[\mathbf{n}] = J^{-1}\log(s_1[\mathbf{n}, J]/s_1[\mathbf{n}, 0])$, where we set $J = 80$. Although this estimation is noisy and inaccurate, we still gain a little improvement in the reconstruction by compensating the $T_2^*$ decay.

Next we propose a reconstruction method based on $\ell_1$ and $\ell_2$ norms, which attempts to decouple inhomogeneity distortion.

## 3. RECONSTRUCTION

Having the low-resolution shift-corrected MRSI data $s[n_x, n_y, n_t]$ with resolution $(\mathbf{M}, N_t)$, we wish to reconstruct $r[\mathbf{n}, n_t] = r[n_x, n_y, n_z, n_t]$ on a higher grid $(\mathbf{N}, N_t)$, which has the same spatial resolution as the estimated field map $\phi[\mathbf{n}]$ (and $T_2^*$ decay). In fact, we reconstruct the volume in multiple slices and then take the average along $n_z$. The reconstruction criterion that we propose in our model is

$$\mathcal{A}r[\mathbf{n}, n_t] = s[n_x, n_y, n_t], \tag{2}$$

where $\mathcal{A}$ is a set of operators simulating the system model (explained later), which makes the desired signal $r[\mathbf{n}, n_t]$ dependent on the field map and $T_2^*$ decay; then generates a lower-resolution volume $s[n_x, n_y, n_t]$ in one slice by taking the center of *k*-space at $(M_x, M_y, N_t)$ resolution.

We propose the following minimization to compensate for the field map and $T_2^*$ decay distortions from acquired signal $s$

$$\tilde{r} = \arg\min_r \left\{ \left\| \mathcal{A}r - s \right\|_{\ell_2}^2 + \lambda_1 \left\| \Delta_{xy} r_{(t)} \right\|_{\ell_1} + \lambda_2 \left\| \Delta_z r_{(t)} \right\|_{\ell_2}^2 + \lambda_3 \left\| r_{(t)} \right\|_{\ell_1} \right\}. \tag{3}$$

Here $\mathcal{A} = \mathcal{W}\mathcal{B}$ composed of two main operators $\mathcal{B}$ and $\mathcal{W}$. The first operator models the scanner for the field inhomogeneity and $T_2^*$ decay distortions. We can formulate $\mathcal{B}$ as

$$r^{\mathcal{B}} = \mathcal{B}r, \tag{4}$$

where $r^{\mathcal{B}}[\mathbf{n}, n_t] = e^{n_t(T_2^*[\mathbf{n}] + j\phi[\mathbf{n}])} r[\mathbf{n}, n_t]$ ($\mathbf{0} \le \mathbf{n} < \mathbf{N}$, $0 \le n_t < N_t$), which distorts $r$ with an exponential term.

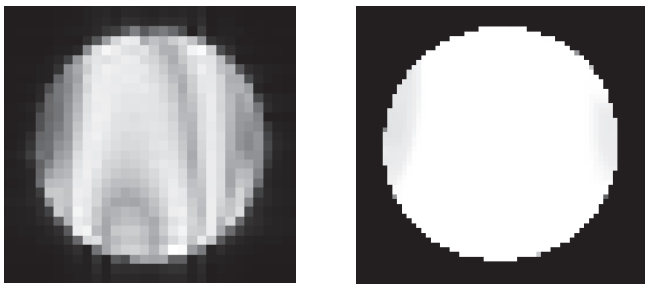

Fig. 3. Spectral peak at $k_t = 0$ for the synthetic data. *Left:* Result of the standard method (zoomed to mach the right figure). *Right:* The resulting spectral peak using the proposed method.

The second operator $\mathcal{W}$ involves a number of Fourier and windowing operations as defined below:

$$r^{\mathcal{W}} = \mathcal{W}r = \mathcal{F}^{-1}_{(xyz)}\mathcal{K}\mathcal{F}_{(xyz)}r\,, \qquad (5)$$

where $\mathcal{K}$ denotes the windowing operation which takes the center part along $[k_x, k_y, k_z]$. Therefore, $\mathcal{W}$ results in shrinking the spatial resolution from $(N_x, N_y, N_z)$ to $\mathbf{M} = (M_x, M_y)$.

There are 3 regularization terms in (3). The first term denotes $\ell_1$ norm of 2-D finite difference [equivalent to *total variation* (TV)] along $[n_x, n_y]$ in the spectral domain, which is required for a high-quality reconstruction of the spectral peaks and is defined as $\left\|\Delta_{xy} r_{(t)}\right\|_{\ell_1} = \sum_{n_x,n_y}\sqrt{\left|\Delta_x f\right|^2 + \left|\Delta_y f\right|^2}$, where $\Delta_x r_{(t)} = r_{(t)}[\mathbf{n}, k_t] - r_{(t)}[n_x - 1, n_y, n_z, k_t]$ and similarly for $\Delta_y r_{(t)}$. By second term we minimize the difference among slices since we assume that the slab that we scan for MRSI is uniform along $n_z$.

In MRSI of a phantom containing metabolites the spectral peaks appear as spikes along $k_t$ while the baseline is flat and noisy. In view of this we propose to minimize $\ell_1$-norm of the spectroscopic data as appears in the third term which has a similar effect to soft thresholding in denoising.

An issue for the minimization algorithms is how to select the regularizing parameters. In our framework of (3), we found by trial and error that by setting $\lambda_3$ to zero, we can fix $\lambda_1 = \lambda_2$ for a desired reconstruction error defined as $e = \left\|\mathcal{A}r - s\right\|_{\ell_2} \Big/ \left\|s\right\|_{\ell_2}$ and then set $\lambda_3$ to a smaller value $\lambda_3 \le 0.1\lambda_1$. In fact, the first two regularizing parameters specify the overall reconstruction quality of the MRS data while the third one removes the spectral noise. Using a high value of $\lambda_3$ would make the peaks non-uniform and degrade the result.

To solve (3), we employ conjugate gradient iterative algorithm [8] along with the prevailing iterative reweighting algorithm [4] to achieve $\ell_1$ norm. In this algorithm at iteration $i+1$ we minimize the following quadratic expression using the conjugate gradient

$$r^{i+1} = \arg\min_r \left\{\left\|\mathcal{A}r^i - s\right\|_2^2 + \lambda_1\left\|q_1\Delta_{xy} r^i_{(t)}\right\|_2^2 + \lambda_2\left\|\Delta_z r^i_{(t)}\right\|_2^2 + \lambda_3\left\|q_3 r^i_{(t)}\right\|_2^2\right\}$$

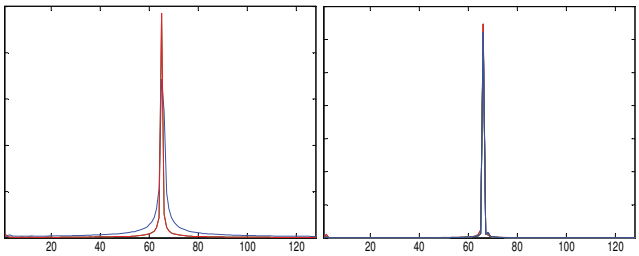


Fig. 4. *Left:* Two examples of spectral peaks using the standard method. *Right:* Same peaks shown in the left reconstructed using the proposed method.

where we employ the weights $q_1[\mathbf{n}, k_t]$ and $q_3[\mathbf{n}, k_t]$ using the previous iteration result:

$$q_1^2[\mathbf{n}, n_t] = \frac{1}{\left|\Delta_{xy} r^i_{(t)}[\mathbf{n}, k_t]\right| + \varepsilon} \quad \text{and} \quad q_3^2[\mathbf{n}, n_t] = \frac{1}{\left|r^i_{(t)}[\mathbf{n}, k_t]\right| + \varepsilon}.$$

We set the initial values as $q_1 = q_3 = \mathbf{1}$ and $r^0 = \mathbf{0}$.

## 4. EXPERIMENTAL RESULTS

### 4.1. Simulation

To test our proposed reconstruction scheme, first we performed a simulation in which we considered $r[\mathbf{n}, n_t]$ with resolution $(64, 64, 4, 128)$ to be all ones within a mask and zero elsewhere (hence $r_{(t)}[\mathbf{n}, k_t]$ has a uniform constant peak at $k_t = 0$ and is zero elsewhere). We assumed $\phi[\mathbf{n}]$ and $T_2^*$ estimations to be the same as the ones we obtained from real data (see Section 2.1). Then we synthetically generated $s[n_x, n_y, n_t]$ with resolution $(\mathbf{M}, M_t) = (32, 32, 128)$ by applying the operator $\mathcal{A}$: $s = \mathcal{A}r$.

We applied our algorithm to reconstruct $r[\mathbf{n}, n_t]$ where we set $\lambda_1 = \lambda_2 = 1$, and $\lambda_3 = 0.1$. We used 45 iterations for the conjugate gradient and applied 10 iterations to the reweighting algorithm. For this set of regularization parameters ($\lambda$'s) we obtained a small reconstruction error of $e = 0.17\%$.

We also reconstructed the data using the standard algorithm where we shift the spectral peaks of $s_{(t)}[n_x, n_y, k_t]$ along $k_t$ in order to align the peaks. This standard method is the conventional scheme to compensate for the field inhomogeneity in MRSI.

Fig. 3 shows the resulting spectral peak image of the reconstructed signal. While our proposed method almost perfectly reconstructed the peak, the standard method shows a poor performance. An example of 2 reconstructed spectral peaks is shown in Fig. 4. The reconstructed peaks using the proposed method are all coincident to the original one within a very small error, but the peaks resulted from the standard method have different magnitudes at $k_t = 0$ and are nonzero for a range of nonzero $k_t$. This simulation indicates the efficiency of our proposed approach in compensation of the field map when the field map estimation is perfect.

### 4.2. Uniform Metabolite Phantom

In addition to the synthetic data simulation that proved the efficiency of our proposed scheme, we also tested the

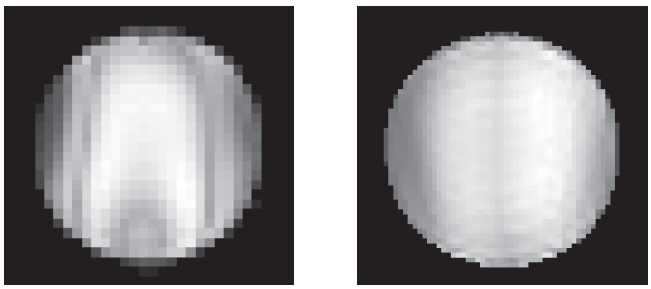

Fig. 5. *Left:* $^1$H spectral peak using the standard method (zoomed version is shown). *Right:* The resulting spectral peak using the proposed method (peak averaging over two frames is used).

reconstruction algorithm on the real MRSI data. We acquired low-resolution metabolite scans with and without water suppression as explained in Section 2.1. First, we reconstructed spectral data for the $^1$H (water unsuppressed) case using the same regularization parameters.

Here we also used the standard method of spectral peak adjustment for comparison. Fig. 5 shows the water spectral peak obtained using the proposed and standard schemes. The proposed reconstruction approach shows superior performance in removing the inhomogeneity distortion.

Next we employed our method for reconstruction of metabolite spectral data where we achieved a reconstruction error of $e = 4.3\%$ . We also applied the standard method using the same shift we obtained from water imaging set for peak alignment. For both methods we applied baseline suppression after reconstruction and for the standard method we applied spectral apodization using a Gaussian window.

In Fig. 6 we depicted Cho, Cr, and NAA reconstructed peaks. Due to chemical shift artifact, the peaks appear in multiple frames, thus we used peak averaging over three frames. The proposed method provides more uniform and smoother spectral images.

Finally, we demonstrated some spectral peaks in Fig. 7. It is clear that the reconstructed peaks using the proposed method are more aligned, less noisy, and more uniform. Classical methods such as LCModel [9] that rely on narrow spectral peaks in order to reconstruct them would not be very efficient for the peaks in our example [Fig. 7(*left*)].

## 5. CONCLUSION

In this work we proposed to use a high resolution field map estimation in order to compensate for the inhomogeneity and reconstruct MRSI data. We proposed a combined $\ell_1$ and $\ell_2$ reconstruction scheme. We showed the superior results of our method when compared to the standard method.

## 6. REFERENCES


[1] W. Du, Y.P. Du, X. Fan, M.A. Zamora, and G.S. Karczmar, "Reduction of spectral ghost artifacts in high-resolution echo-planar spectroscopic imaging of water and fat resonances," *Mag. Res. Imaging*, vol. 49, pp. 1113-1120, 2003.

[2] A. Ebel and A.A. Maudsley, "Improved spectral quality for 3D spectroscopic imaging using a high spatial resolution acquisition strategy," *Mag. Res. Imaging*, vol. 21, no. 2, pp. 113-120, 2003.


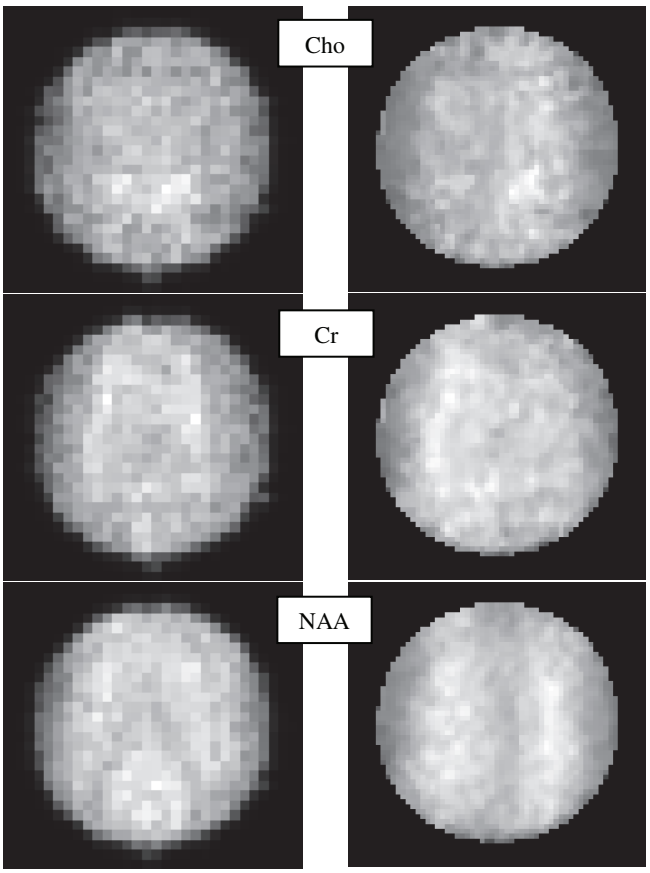


Fig. 6. *Left:* Spectral peaks using the standard method. *Right:* The resulting peaks using the proposed method. Peak averaging over three frames is used.

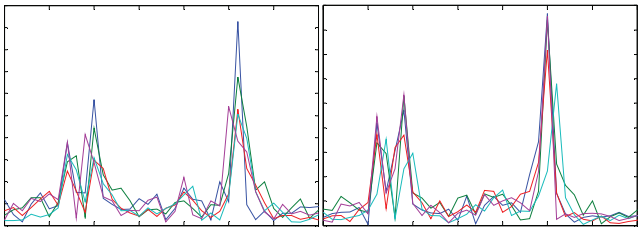

Fig. 7. Some reconstructed spectral peaks corresponding to Cho, Cr, and NAA. *Left:* The standard method. *Right:* The proposed method.


[3] A. Funai, J.A. Fessler, D. Yeo, V. Olafsson, and D. Noll "Regularized field map estimation in MRI" *IEEE Trans. Medical Imaging*, vol. 27, no. 10, pp. 1484-1494, Oct. 2008.

[4] I.F. Gorodnitsky and B.D. Rao, "Sparse signal reconstruction from limited data using FOCUSS: A reweighted norm minimization algorithm," *IEEE Trans. Signal Processing*, vol. 45, pp. 600-616, Mar. 1997.

[5] M. Jacob, X. Zhu, A. Ebel, N. Schuff, and Z.-P. Liang, "Improved model-based magnetic resonance spectroscopic imaging," *IEEE Trans. Medical Imaging*, vol. 26, no. 10, pp. 1305-1318, Oct. 2007.

[6] I. Khalidov, D. Van De Ville, M. Jacob, F. Lazeyras, and M. Unser, "BSLIM: spectral localization by imaging with explicit B0 filed inhomogeneity compensation," *IEEE Trans. Medical Imaging*, vol. 26, no. 7, pp. 990-1000, Jul. 2007.

[7] Z.-P. Liang and P.C. Lauterbur, *Principles of magnetic resonance imaging: A signal processing perspective,* IEEE Press, New York, 2000.

[8] J. Nocedal and S.J. Wright, *Numerical optimization,* 2nd Ed., 2006.

[9] S.W. Provencher, "Estimation of metabolite concentrations from localized *in vivo* proton NMR spectra," *Mag. Res. Med.* vol. 30, pp. 672–679, 1993.